Seasonal and tidal variability of the hydrology and suspended particulate matter in the Van Uc estuary, Red River, Vietnam

Violaine Piton, Sylvain Ouillon, Vu Duy Vinh, Gael Many, Marine Herrmann, Patrick Marsaleix

Seasonal and tidal variability of the hydrology and suspended particulate matter in the Van Uc estuary, Red River, Vietnam

Violaine Piton[1,2], Sylvain Ouillon[1,2], Vu Duy Vinh[2,3], Gaël Many[4], Marine Herrmann[1,2], Patrick Marsaleix[4]

[1] LEGOS, IRD, UMR556 IRD/CNES/CNRS/Université de Toulouse, 31400 Toulouse, France

[2] LOTUS Laboratory, University of Science and Technology of Hanoi (USTH), Vietnam Academy of Science and Technology (VAST), 18 Hoang Quoc Viet, Cau Giay, Hanoi, Vietnam

[3] Institute of Marine Environment and Resources, VAST, Haiphong city, Vietnam.

[4] LA, CNRS, Université de Toulouse, 31400 Toulouse, France

Corresponding author: violaine.piton@legos.obs-mip.fr

Submitted to Estuaries and Coasts.

Abstract

This study explores the seasonal and tidal changes in flow and suspended matter dynamics in the tropical and macrotidal Van Uc River estuary (North Vietnam) and aims at understanding, among others, the sediment delivery to the ocean and the processes behind the estuary siltation. Four campaigns took place during the contrasting high flow and low flow seasons, for each during neap and spring tides. Water and suspended matter fluxes, salinity, turbidity and suspended sediment concentrations were measured for 24h at three cross sections along the estuary. During the high-flow season, the estuary was mixed, with seaward sediment flux during neap tide and ephemeral up-estuary sediment flux at spring tides due to tidal distortion. During the low-flow season, the system transitioned from partially mixed to highly stratified with salty waters intrusions, salt wedge presence and up-estuary sediment flux varying with the tidal regime. Estuarine siltation mostly occurred during low-flow at spring tides with a suspended matter inflow, primarily due to local resuspension, which represented ⅔ of the outflow. These findings also provide a new benchmark for hydro-sedimentary model calibration/validation.

Keywords: suspended sediments, estuary, estuarine turbidity maximum, neap/spring cycle, Red River, Vietnam

1. Introduction

Estuaries are links between land and ocean where freshwater coming from the rivers mixes with saline oceanic water (Wolanski et al., 2013). They are typically characterized by strong gradients of salinity, temperature, water surface level and suspended sediment concentrations (Priya et al.,

2012; Jay et al. 2014), and contribute to a high amount of sediments, nutrients and contaminants input to the ocean (Milliman, 1991; Meybeck, 1993). These transitional zones are never at a steady state, experiencing a variability at longer time scale from the river basin (interannual to seasonal) than from the ocean. Since the effects of tidal currents on the salt and momentum balances in estuaries were recognized by Pritchard (1954, 1956), tides indeed are known to play a key role in estuarine dynamics. Affecting mixing, influencing a stronger or weaker stratification depending on the sea water intrusion, and determining the characteristics of the water masses that can interact with the shelf circulation, tidal and neap-spring cycles are amongst the main drivers of estuarine dynamics (Geyer and MacCready, 2014). In some cases, estuarine waters may appear being well-mixed during flood and being stratified during ebb (Simpson et al., 1990; Jay and Smith, 1990a). Also, the residual circulation, the turbulent mixing (Simpson et al., 1990; Geyer et al., 2000) and the along-estuary circulation (Lai et al., 2018) appeared to vary in response to the spring-neap cycle.

The evolution of the Red River delta in terms of siltation, erosion and accretion of its estuaries and coastlines constitute a major concern, as the delta is the most populated region of Vietnam, and is the second-most important rice-producing region of the country. The Red River was ranked as the ninth river in the world in terms of sediment discharge but the construction of two dams across the river in the 1980s caused a reduction of sediment discharges from 145-160 Mt y^{-1} in the 1970s (Milliman and Meade, 1983) to 40 Mt y^{-1} nowadays (Le et al., 2007; Vinh et al. 2014; Wei et al., 2019). Changes in water regulation due to the dams, induced an increasing siltation of the harbour of Hai Phong, which is the second biggest harbour of the country and connects northern Vietnam to the world market. Such phenomenon forces an increasing dredging

effort each year, with 6.6 million US $ spent on dredging activities in 2013 (Vietnam maritime administration 2017). Recent studies have arisen from this issue, and the tidal pumping has been pointed out as one of the physical processes responsible for the siltation, by creating a net upstream transport of sediments in the dry season, which settled in a near bed layer at low turbulent energy (Lefebvre et al., 2012). In the Cam-Nam Trieu estuary, the Estuarine Turbidity Maxima (ETM, mass of highly concentrated suspended sediments) was shown to start developing at salinities as low as 0.1 PSU (Vinh et al., 2018) and bio-aggregation was shown to be enhanced at salinity around 10-15 PSU due to increasing stickiness properties of bio-exopolymeric substances (Mari et al., 2012). In the coastal zone, the decrease of the suspended sediment loads caused alternative patterns of erosion and accretion to develop. For example, the Ba Lat River mouth (Fig. 1) has expended seaward due to a combined effect of sediment resuspension by wave actions and river floods (van Maren et al., 2007), and increased turbidity was observed in the touristic region of Do Son, while Hai Hau coasts have experienced a severe erosion of several meters per year. In this context, investigating the fine scale physical processes in estuaries and in their regions of influence is of particular interest for better understanding the Red River system.

The Van Uc River (Fig. 1) is a typical distributary of the Red River, with rice crops all along the banks that require water and construction of soil dykes for flooding protection, and with constant river bed dredging for both navigable waterways and selling purposes. It is ranked at the third position of the Red River system in terms of both water and sediment discharges. (Vinh et al., 2014). Above all, the Van Uc estuary is an interesting site to study estuarine dynamics because

this meso- to macrotidal estuary (maximum tidal range: 4m) is both influenced by a strong seasonal river signal and a monsoon regime. Using the MIKE11 numerical model, Vinh et al. (2014) estimated that 70 % of the annual water discharges were issued in the wet season (June-October) while 16 % were issued in the dry season (December-April), the 14 % remaining being issued in intermediate periods (May and November). For the sediments discharges, 86 % of the total annual discharges were issued in the wet season, against 4 % in the dry season (10% were issued in the intermediate seasons). If seasonal budgets of water and sediments are globally known, forced by the river inputs (Vinh et al., 2014), if seasonal variations of hydrology (water flux, salinity, stratification) and suspended matter was described at one station in the Ba Lat river mouth (Fig. 1) (van Maren, 2004) and if transects along the estuaries of the Red River distributaries were described at different seasons at spring tides (Vinh et al., 2018), no effort has been initiated so far to document the hydrology and the suspended matter dynamics of Red River estuaries in terms of tidal variability. This question represents the central objective of the present study, which aims at documenting the lack of knowledge regarding the hydro-sedimentary processes in the Red River.

Based on new in situ data, this paper focuses on the analysis of the hydrology and on the characteristics of the suspended particulate matter at different seasons and tidal cycles, along the Van Uc estuary. It is the first step of a more comprehensive modeling study that aims at further analyze the transport and fate of sediments from the Red River to the Gulf of Tonkin, using the hydrodynamical-sediment transport model SYMPHONIE-MUSTANG (Marsaleix et al., 2008;

Le Hir et al., 2011) that is configured for the region. Hence, the choice of the parameters studied was made in a modelling perspective.

In Section 2, the estuary of interest is presented and in Section 3, field campaigns and methodologies for data sampling, instruments calibrations and data analyses are described. In Section 4, findings on water and sediment fluxes, water column stratification and particles properties, which are largely impacted by the lunar tidal cycle and related circulation are detailed. The dynamical mechanisms that can explain these results are discussed in Section 5: in particular the distinct effects of gravitational circulation and of the along-estuary tidal distortion on sediment fluxes and deposition.

2. Regional settings - The Van Uc estuary

The Van Uc estuary is located next to Hai Phong city (the third largest city of Vietnam), northeast of Vietnam (Fig. 1). The estuary is fed with fresh water and sediments by the Van Uc river, one of the nine distributaries of the Red River, which receives water and sediments from both the Red River, through the Duong River, and from the Thai Binh River through a complex network of connections within the Red River Delta (see Vinh et al., 2014). The total river discharge through the Van Uc estuary was estimated of about 17.7×10^9 m^3 y^{-1} (for the period 1989-2010), which corresponds to 14.5 % of the total water discharge from the Red-Thai Binh system to the Gulf of Tonkin (Vinh et al. 2014). These authors also evaluated the sediment fluxes and found a drastic drop in the annual fluxes due to the Hoa Binh dam impoundment in the 1980s (from 11.5 to 5.1 Mt y^{-1}). The Van Uc sediment flux represents 14.4 % of the total

sediment flux of the Red-Thai Binh River to the Red River coastal area and is therefore the third most important distributary of the Red River Delta in terms of river and sediment discharges (after the Day and the Ba Lat rivers).

The Van Uc estuary is subjected to the South-East Asian sub-tropical monsoon climate (Wyrtki 1961), that is characterized by an alternation of a southwest summer monsoon and a northeast winter monsoon. The wet summer season (June to September) accounts for 85-95% of the total annual rainfall in the region (~1161 mm) and is dominated at 72% by winds blowing from the South-West. In the dry winter season, the winds blow at 92% from the North-East and bring cold and dry conditions over the region (Vinh et al., 2018). The seasonal variation of the Red River hydrological regime is therefore strong and largely influences the Van Uc estuary. Vinh et al. (2014) showed that 71-79% of the annual total water discharge of the Van Uc River was brought to the coastal zone during the wet season and only 9-18% in the dry season (December to March).

The South China Sea and the Gulf of Tonkin are one of the few regions in the world where diurnal tides dominate the semidiurnal tides (Fang, 1986). Wyrtki (1961) was the first to identify the main tidal constituents in the South China Sea: O1, K1, M2, S2 (classified by their importance in amplitudes). The diurnal tide dominates due to a double resonance : in the South China Sea because of Helmholtz resonance (Zu et al., 2008), then in the Gulf of Tonkin, higher for O1 than K1 due to a resonant peak period of 29h (Nguyen et al., 2014). The tide gauge measurements next to the Van Uc River mouth (at Hon Dau, Fig. 1) show a tidal amplitude of about 0.5-1.0 m in neap tides and of about 2.6-3.6 m in spring tides.

3. Material & Methods

3.1 Field data and sampling procedure

Four field surveys were performed in the Van Uc estuary during neap and spring tides in the wet and dry seasons. Surveys are noted WN for wet season at neap tide, WS for wet season at spring tide, DN and DS for surveys in the dry season at neap tide and spring tide, respectively. The dates of each survey with corresponding tidal cycles and seasons are listed in Table 1.

Three stations (ST1, ST2 and ST3) spaced by 10 km were selected for sampling (Fig. 1). ST1 is located next to the river mouth while ST3 is the further upstream. Each station was sampled during 24 hours with cross-river transects measurements every two hours to cover a full diurnal cycle, starting at ST1 and finishing at ST3. Each series of measurements consisted of four different steps. Firstly, cross river velocity profiles were measured with a hull-mounted, downward-looking, 1200 kHz Acoustic Doppler Current Profiler (ADCP RDI Workhorse in bottom tracking mode). Current magnitude and direction were measured in depth cells of 0.25 m with a range of 15 m using a frequency of 0.2 Hz. Secondly, vertical profiles of conductivity and temperature were measured for each transect, in the deep channel at the middle of the river, using a profiling CTD Compact-CTD (ASTD687, Alec Electronics Co., Nishinomiya, Japan, now released by JFE Advantech Co., Nishinomiya, Japan, as Rinko-Profiler). Thirdly and parallel to CTD measurements, depth profiles of floc size distribution and concentration were measured using an in situ laser scattering and transmissometry instrument with a 90% path reduction module (LISST-100X, type B, Sequoia Scientific Inc., Bellevue, WA, USA). The LISST-100X

determines the volumetric particulate concentration in 32 logarithmically spaced size classes from 1.25 to 250 µm and uses a red laser (660 nm) through a path of 5 cm with a sampling rate of 1 Hz. In order to study the relationship between turbidity and suspended particulate matter concentration, water samples (of ~ 1 l) near subsurface (at ~1.5 m depth) were also collected every four hours (i.e. every two CTD deployments) with a Niskin bottle. Turbidity of these samples were measured onboard using a Hach 2100Q Turbidimeter.

Data at the hydrographic station Trung Trang (Fig. 1), provided by the National Hydro-Meteorological Service (NHMS), were also used in this study. They include hourly water discharges and water elevations.

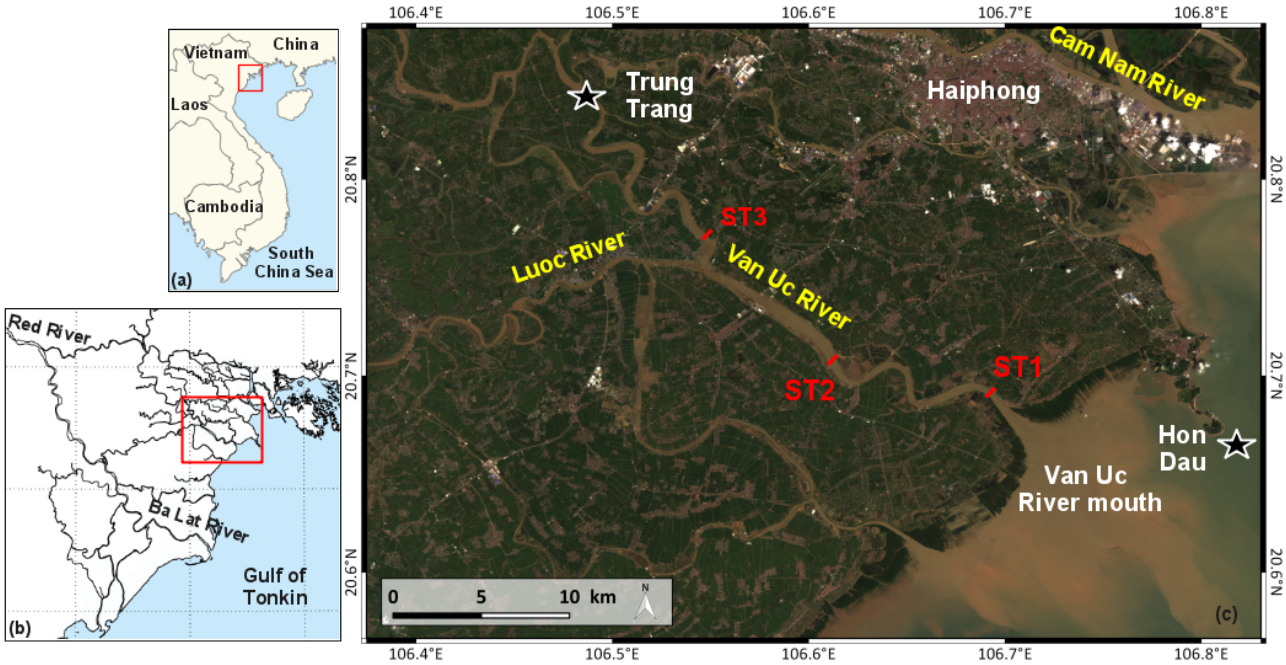

Fig. 1 Location of stations ST1, ST2 and ST3 (in red) in the Van Uc River and of Trung Trang and Hon Dau hydrological stations (black star) (Landsat 8 image from September 29, 2017).

Survey name	WN			WS			DS			DN		
station	ST1	ST2	ST3	ST1	ST2	ST3	ST1	ST2	ST3	ST1	ST2	ST3
Dates (of 2017)	26/08	27/08	28/08	03/09	04/09	05/09	06/12	07/12	08/12	12/12	13/12	14/12
season	wet			wet			dry			dry		
regime	neap			spring			spring			neap		

Table 1: Van Uc surveys characteristics and dates of sampling. Each sampling started at 8 am and finished at 6 am the following day.

3.2 Hydrological parameters

Salinity and density were derived from CTD data (temperature and conductivity) following general UNESCO polynomial relationship (UNESCO, 1983).

The Brunt-Väisälä frequency N^2 (in s^{-2}), also known as the buoyancy frequency, was computed from the density depth-profiles and used as an indicator of the water column stratification:

$$N^2 = \frac{-g}{\bar{\rho}} \frac{\delta \rho}{\delta z} \quad (1)$$

where g is the acceleration of gravity ($m^2\ s^{-1}$) and ρ the potential water density ($kg\ m^{-3}$). A stable stratification is considered when $N^2 > 0$, while a stratification is considered unstable when $N^2 \sim 0$ (Turner, 1973).

The dimensionless Richardson number (Ri), which is used as a criterion for assessing the stability of stratified shear flow through energy consideration, is computed by comparing N^2 to the vertical gradient of the horizontal current velocities ($\frac{\delta V}{\delta z}$) from ADCP data (Pacanowski and Philander, 1981), as:

$$Ri = \frac{N^2}{(\frac{\delta V}{\delta z})^2} \quad (2)$$

When Ri $\geq$ 0.25, the flow is considered stable and if Ri < 0.25, the turbulence overcomes the density stratification and generates vertical mixing (Miranda et al., 2002; Kirinus et al., 2002). Furthermore, the Simpson parameter gives the potential energy ϕ (in J m^{-3}) that represents the mechanical energy required to completely mix the water column. This parameter was used to quantitatively analyze the physical mechanisms contributing to mixing and stratification in an estuary (Simpson et al. 1978) and was computed as follows:

$$\phi = \frac{1}{H} \int_{-H}^{0} gz\,(\overline{\rho} - \rho)\,\delta z \quad (3)$$

with H, the water column depth.

3.3 Water currents and derived water discharges

The ADCP transmits high frequency acoustic signals (pings), that are backscattered from water constituents of different origins: suspended sediment, phyto/zooplankton and bubbles. These constituents are assumed to travel with the speed of water and therefore, the current velocity (horizontal and vertical) and the current direction as a function of depth are estimated through the Doppler effect. Following the recommendations of Mueller et al. (2013), water

discharges (noted $Q_{Measured}$) were computed using the measured water velocities (noted V_w) and the boat velocities (noted V_b):

$$Q_{Bin} = (V_{wu} V_{bv} - V_{wv} V_{bu}) dtdz \qquad (4.a)$$

$$Q_{Measured} = \sum_{j=1}^{Ensembles} \sum_{i=1}^{Bins} Q_{Bin} \qquad (4.b)$$

where V_{wu} and V_{wv} correspond to the meridional and zonal water velocities, respectively, and V_{bu} and V_{bv} correspond to the meridional and zonal boat velocities, respectively. Q_{Bin} (in $m^3 s^{-1}$) was computed for each ensemble (i.e. time between two measurements) *dt* (5 s) and for each vertical bin *dz* (0.25 m). As recommended by Mueller et al. (2013), the total water discharge Q_{ADCP} of the river is the sum of $Q_{Measured}$ and the water discharges estimated in the unmeasured zones by the ADCP (i.e. the top and bottom layers and the right and left edges of the river) as:

$$Q_{ADCP} = Q_{LeftEdge} + Q_{Top} + Q_{Measured} + Q_{Bottom} + Q_{RightEdge} \qquad (5)$$

Detailed descriptions and formulations of $Q_{LeftEdge}$, $Q_{RightEdge}$, Q_{Top} and Q_{Bottom} are available in Mueller et al. (2013) and were computed accordingly.

Furthermore, the flux throughout the water column can flow in opposite directions (downstream or upstream), whether it is dominated by the river flow or by flood tides. Therefore, we chose to compute $Q_{ADCP}+$ as the component of the flux flowing downstream and $Q_{ADCP}-$ as the component of the flux flowing upstream. Note that the sum of $Q_{ADCP}+$ and $Q_{ADCP}-$ is equal to Q_{ADCP}.

3.4 Suspended particulate matter parameters

3.4.1 SPM concentration from water samples

Following the process proposed by Aminot and Kérouel (2004), the suspended particulate matter (SPM) concentrations were determined by filtering onboard a known volume of water (about 100-150 ml) per sample through two kinds of pre-weighed filters: polycarbonate Nuclepore filters (porosity 0.45 µm) and Whatman GF/F glass microfiber filters (porosity 0.7 µm). After filtration, filters were rinsed three times with 5.0 mL of milli-Q water to remove salt. Then, they were dried for 24 hours at 70°C in an oven and weighed on a high-precision electrobalance. The sediment concentration obtained after drying the filters is the total SPM concentration, called $SPM_{Filters}$ hereafter, including organic and inorganic matter.

The particulate inorganic matter concentration was measured after burning the GF/F filter at 450 °C during 4 hours: this process removes all the organic matter from the filter. The difference between the total $SPM_{Filters}$ and particulate inorganic matter provided the particulate organic matter concentration and thus the ratio of organic to inorganic matter (particulate organic matter/particulate inorganic matter) within the $SPM_{Filters}$.

3.4.2 Optical backscattering sensors (OBS)

Turbidity is an optical proxy of SPM concentration which is measured by nephelometers or optical backscattering sensors (OBS). The CTD was equipped with an OBS measuring in the

infrared. The sensor outputs (in Formazin Turbidity Unit - FTU) were calibrated against gravimetric SPM concentrations measurements. The SPM concentrations measured by the CTD are called hereafter SPM_{OBS}.

3.4.3 ADCP's backscatter index

For the past twenty years, acoustic instruments such as ADCP, originally designed to measure velocity profiles, have been used to quantify SPM concentrations in ocean and coastal environments (Thorne and Hanes, 2002; Tessier et al., 2008; Le Coz et al., 2009). The measurement principle is based on the fact that the acoustic signal is emitted with an initial intensity, that progressively decreases as it travels through the water column, and which is backscattered by suspended particles. Therefore, the intensity of the backscattered acoustic signal is a function of the quantity of the particles present in suspension in the environment. The acoustic method has the advantage of being non-intrusive.

In order to infer the particle load from the signal recorded by the ADCP, the sonar equation (in dB) was used. The sonar equation represents an energy balance that expresses a signal-to-noise ratio, taking into account the technical characteristics of the instrument. The received acoustic level (RL), can be expressed as follows (Deines, 1999; Lurton, 2002):

$$BI = RL + 2TL - SL \qquad (6)$$

with SL, the source level emitted by the ADCP (in dB), TL the transmission loss due to attenuation of the acoustic wave within the ambient environment (in dB), and BI the backscatter index, which depends on the SPM concentration.

In our case and following the recommendation of Mullison (2017), the RL was computed as follows:

$$RL = 10log\,(10^{Kc\,(E-Er)/10} - 1) + Br \qquad (7)$$

where Kc (in dB/counts) is the factor used to convert the amplitude reported by the ADCP, in counts, to decibels. E the backscattered intensity of the acoustic wave, which was measured by the instrument (in counts), Er the backscattered intensity signal, which is seen by the instrument in the absence of any signal (the noise) and Br, the associated pressure level furnished by the manufacturer (dB). In our case, since we will be looking at relative SPM concentrations, neglecting Br will not affect our results.

Two types of transmission losses can be estimated. One is associated to the spherical spreading, which corresponds to the decrease of the signal intensity as the signal travels away from the emission source. The other type of loss corresponds to the acoustic signal attenuation due to the ambient environment, i.e. the attenuation due to the water (α_w) and the attenuation due to the suspended particles characteristics (α_s). In the presence of particles, the total transmission loss, with a distance R from the emission source and ϕ the beam angle (20°), is expressed as follows:

$$TL = 20log_{10}(\frac{R}{cos(\phi)}) + \int_0^R (\alpha_w(r) + \alpha_s(r))\,dr \qquad (8)$$

The attenuation coefficient α_w (dB m^{-1}) was estimated from the model of François and Garrison (1982a, 1982b). According to Tessier (2006), the particle attenuation α_s becomes significant

when the SPM concentration is of the order of 200 mg l^{-1} for a 1200 kHz acoustic signal and fine particles. The concentrations of SPM measured during the surveys (estimated from CTD OBS profiling) were rather low in the dry season, and never exceeded 170 mg l^{-1} in the wet season. Therefore, the choice was made to neglect α_s in the calculation of the backscatter index (BI).

An accurate estimate of the acoustic source level (SL) emitted by the ADCP is difficult. It can either be obtained by laboratory calibrations of the instrument, or by using the average reference values provided by the manufacturer. Laboratory experiments showed that for a 1200 kHz ADCP, the values range from 216 to 218 dB (Tessier, 2006). Furthermore, the SL can vary with the battery voltage. This effect could infer a bias in the measurement, when using the manufacturer reference. In our case, the ADCP was not calibrated prior to the survey, and therefore SL is neglected. Again, since we only look at relative SPM concentrations, neglecting SL does not alter our results.

Lastly, the best regression relationship between SPM concentrations measured by optical backscattering (SPM_{OBS}) and BI is found to be linear between $10log_{10}$(SPM) and BI. It is used to estimate SPM concentrations (in mg l^{-1}) from acoustic measurements (in dB), called SPM_{AC} hereafter, following:

$$10log_{10}(SPM_{AC}) = aBI + b \qquad (9)$$

with *a* and *b* the slope and the intercept of the linear regression.

However, the uncertainties associated with the different terms of the sonar equation remain important, and the calibration of the acoustic signal is done in practice by adjusting the slope.

3.4.4 Sediment discharges from ADCP

For each ensemble *dt* (5 s) and vertical bin *dz* (0.25 m), the sediment discharge (noted Q_{BinSED}) was computed as the product of instantaneous Q_{ADCP} and SPM_{AC} as:

$$Q_{BinSED} = (Q_{ADCP} \times SPM_{AC})dtdz \qquad (10.a)$$

and the total sediment discharge is then :

$$Q_{SED} = \sum_{j=1}^{Ensembles} \sum_{i=1}^{Bins} Q_{BinSED} \qquad (10.b)$$

Furthermore, $Q_{SED}+$ was computed as the component of the sediment flux flowing downstream and $Q_{SED}-$ as the component of the sediment flux flowing upstream. Note that the sum of $Q_{SED}+$ and $Q_{SED}-$ is equal to Q_{SED}.

3.3.5 Particles properties measurements from LISST

The laser diffraction spectrum, discretized over 32 classes, was first converted into a particulate volume concentration (in µl l^{-1}) using the factory volume calibration constant. The sum of the contributions provided the SPM volume concentration (SPMVC). However, following the recommendation of Mikkelsen et al. (2005), the extreme size classes #1, #2, #31 and #32 were removed before calculating the SPMVC, the particle size distribution (PSD) and

the mean apparent diameter (D_{50}). Indeed, in stratified waters, water masses have different densities and therefore different refractive indexes which can cause significant light scattering. This phenomenon is known and called the schlieren effect. The LISST probe detects the schlieren effect as an accumulation of large or small particles (i.e., the extreme classes of the spectrum) in the pycnocline (Styles 2006; Mikkelsen et al. 2008). In addition, the measurements for which peaks of particles in extreme classes occurred have been removed, as we found that schlieren effect happened to also contaminate classes as high as #4 and as low as #26. Based on data between classes #3 (1.74 μm) and #30 (179.53 μm), the particulate volume concentration was normalized by the width of each logarithmically-spaced class and gave the PSD (in $\mu l\ l^{-1}$ μm). Then, D_{50} (in μm) was calculated as the diameter corresponding to 50% of the cumulative volume concentration of particles.

4. Results

The effects of seasonal, tidal and spatial forcings on various water column parameters were investigated. Water and sediment fluxes are presented in the first part. The second part is dedicated to the hydrology and turbidity of the water column. Lastly, the suspended particulate matter variability is discussed.

4.1 Fluxes

4.1.1 Calibrations of the optical and acoustical SPM, SPM_{OBS} and SPM_{AC}

Calibrations of optical instruments must be carried out in environments where flocculation of fine grains/particles occurs and where hydrodynamics and grain types/particles properties are highly variable (Bunt et al., 1999). A linear regression was used between the OBS signal (i.e. the turbidity, in FTU) and the filtered $SPM_{Filters}$ concentration (in mg l^{-1}), for the wet season surveys and for the dry seasons surveys. The slope (a) and the intercept (b) of the fitted regression lines were a=0.90 and b=-9.84 for the wet season (R^2=0.96), and a=1.08 and b=-3.86 for the dry season (R^2=0.88). Based on these relationships, SPM_{OBS} concentrations were determined from the turbidity profiles, for each season.

The best-fit regression relationship between SPM_{OBS} and BI was used at each survey to derive SPM concentrations SPM_{AC} from the acoustic signal (Fig. 2). The correlation coefficient R^2 reflects the different sensitivity of optical and acoustic sensors to changes in SPM size and characteristics/properties. Indeed, backscattering is influenced by sediment type, size, color and composition, with optical and acoustical backscattering showing different sensitivities and responses to these parameters (Thorne et al., 1991; Fugate and Friedrichs, 2002; Voulgaris and Meyers, 2004; Downing 2006). Gartner and Cheng (2001) and Gartner (2002) showed that optical sensors are more sensitive to small particles while acoustic sensors are more sensitive to large particles. Furthermore, Kim and Voulgaris (2003) found a slight bias in the SPM_{AC} estimates when the sediment is silt or finer. Rouhnia et al. (2014) showed that the intensity of the backscattered acoustic signal from flocs is mainly affected by the flocculi (i.e the microflocs). However, flocs can have a smaller influence on the backscatter signal than sand grains of the

same size, due to their lower density (Ha et al., 2011). Therefore, the SPM_{AC} should be considered with caution and as estimates only, rather than exact SPM measurements.

Good correlations between SPM_{OBS} and BI were found for surveys WN, WS and DS with R^2 of 0.83, 0.84 and 0.70, respectively (Fig. 2 a, b, c). Only survey DN showed a poor correlation (0.04) between the datasets (Fig. 2 d). Following the circulation and thermohaline conditions of the water column in survey DN (Fig. 3 and see section 4.2), the water column was, at some specific tidal stages, divided in two water masses flowing in opposite direction. The choice was made to compute different calibrations for the top and bottom layers, and the boundary between the two layers was defined by the reversal in current direction. A good correlation was found for the bottom layer (0.85) (Fig 2 f), but a poor correlation remained in the top layer (0.13) (Fig. 2 e). Therefore, for this particular case (top layer of the water column, survey DN), SPM_{AC} could not be estimated. As a first guess and instead of using Eq. 10 b., the contribution of this layer to the sediment discharge Q_{SED} was computed as the product of the mean SPM_{OBS} with the mean Q_{ADCP} of the top layer of the water column. Results of these estimates are presented in the following section.

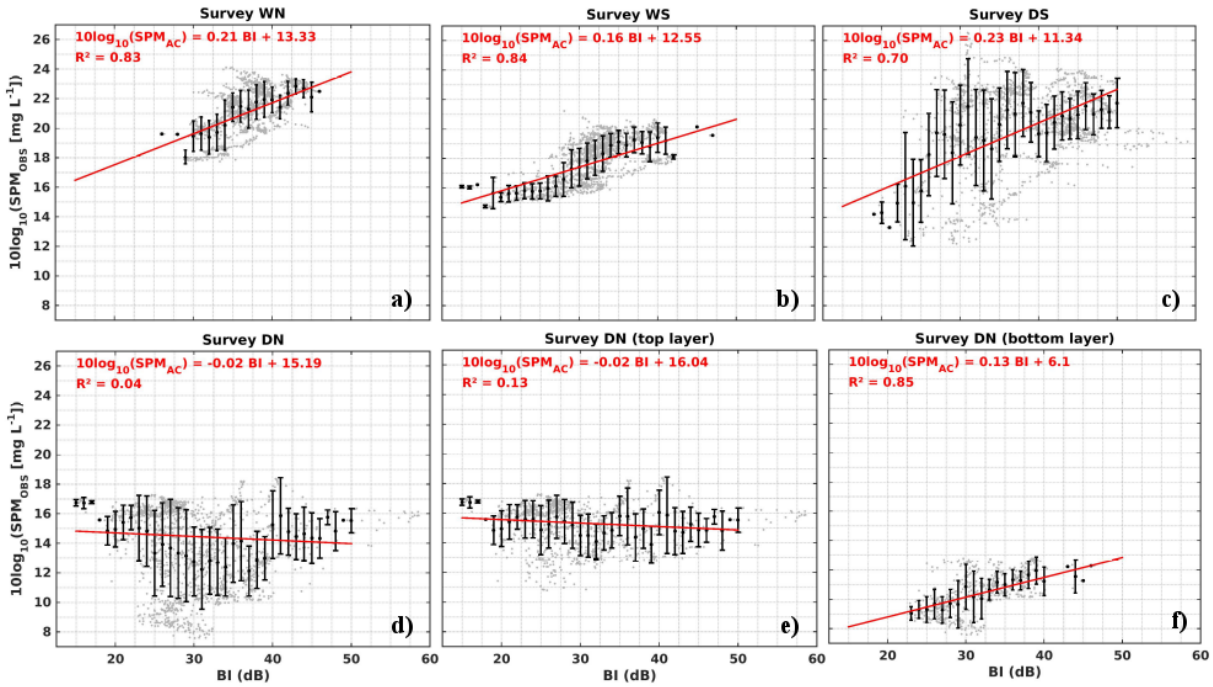

Fig. 2 $10\log_{10}$ of suspended matter concentration estimated from CTD OBS (SPM_{OBS} in mg l^{-1}) against the ADCP backscattering index (BI in dB) for each survey WN, WS, DS and DN (panels a, b, c, d respectively). Raw data are shown in grey and the binned data in black, the data trend line is shown in red. Panels e and f correspond to the top and bottom water layers respectively in survey DN. On the y-axis, 10 corresponds to 10 mg l^{-1}, 16 to 40 mg l^{-1}, 20 to 100 mg l^{-1}, 26 to 400 mg l^{-1}.

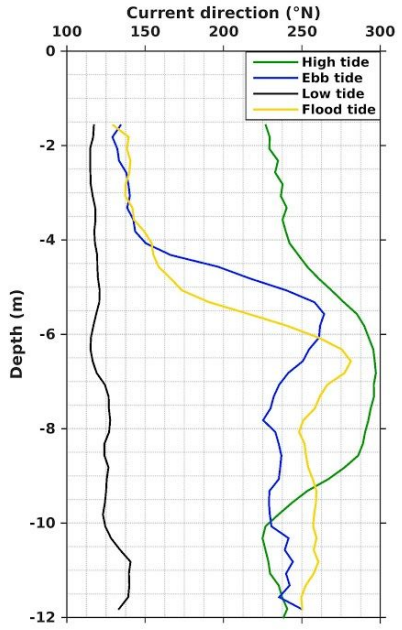

Fig. 3 Mean currents directions (in °N) measured at ST2 during survey DN at high tide (8 am), ebb tide (12 am), low tide (4 pm) and flood tide (2 am).

4.1.2 Water and sediment budgets

4.1.2.1 Time variations

Seasonal variations in Q_{ADCP} were high, with wet season water discharges (2425 m^3 s^{-1} in average over the survey WN and 1757 m^3 s^{-1} for survey WS, Table 2) 4 to 11 times larger than the discharges in dry season (478 and 222 m^3 s^{-1} for survey DS and DN, respectively). Suspended sediment discharges Q_{SED} varied accordingly, with 3 to 170 times larger values in wet season than in the dry season (0.34 t s^{-1} in WN and 0.11 t s^{-1} in WS, as compared to 0.04 and 0.002 t s^{-1} in surveys DS and DN, respectively).

During the wet season, the total water and sediment discharges Q_{ADCP} and Q_{SED} were dominantly directed down-estuary (Q_{ADCP}+ and Q_{SED}+) and only very limited fluxes directed up-estuary (Q_{ADCP}- and Q_{SED}-) were observed (Fig. 4 a,b ; Table 2). In neap tide, a mean Q_{ADCP}+ of 2432 m^3 s^{-1} was measured against a mean Q_{ADCP}- of 7 m^3 s^{-1}, the associated mean Q_{SED}+ being of 0.34 t s^{-1} against a mean Q_{SED}- of 10^{-4} t s^{-1}. In spring tide, up-estuary fluxes were slightly higher but less than 4% of the total water and sediment discharges (Table 2).

As expected, the up-estuary component of the water discharge (Q_{ADCP}-) was much higher in the dry season than in the wet season (Table 2). During the dry season, both down-estuary and up-estuary flows contributed to the total water and sediment fluxes. Globally, the down-estuary water and suspended sediment discharges were respectively 61 and 66% higher than the up-estuary water and suspended sediment flows in the dry season (Table 2). The range of Q_{ADCP} was around 3 times higher in spring tide (from -3976 to 3178 m^3 s^{-1}) than in neap tide (from -1252 to 1826 m^3 s^{-1}, Fig 4. c,d). The difference was highly enhanced in the range of Q_{SED} (from -0.55 to 0.45 t s^{-1} in spring tide, while they ranged from -0.015 to 0.022 t s^{-1} in neap tide, Fig 4. c,d).

Fluxes were very sensitive to tidal variations in dry season, and in wet season during spring tide (Fig. 4).

In the dry season and in the wet season at spring tide, Q_{ADCP} was influenced by the tidal diurnal cycle with high discharges at low tides, decreasing discharges at rising tides, low discharges at high tides and increasing discharges at falling tides (Fig. 4 b,c,d). Q_{SED} followed the same patterns.

In the wet season, only spring tides have induced large enough amplitudes (of ~2 m) to balance the riverine discharge and induce up-estuary flow (Q_{ADCP}-) at stations ST1 and ST2 (Fig. 4 b) ; tidal currents at neap tides (maximum amplitudes of 0.5 m) were not strong enough to impact the riverine discharges (Fig. 4 a). The rest of the diurnal cycle (i.e. low, ebb and flood tides) at each station was dominated by a down-estuary flow (Q_{ADCP}+), which increased with ebb tides and was the highest around low tides.

A noticeable difference can be seen on the flow regime between spring and neap tides in dry season. During spring tides, the flow was alternatively strictly down-estuary and strictly up-estuary with positive Q_{ADCP} values and no Q_{ADCP}- component during 12 hours then the reverse during the next 12 hours from the end of flood until halfway through ebb (Fig. 4 d). At neap tides (survey DN, Fig 4 c), the reversion of the total flow also occurred, but was more nuanced with both Q_{ADCP}- and Q_{ADCP}+ components contributing at the same time to the flow at ST1 and ST2. This particular case resulted from the strong stratification at neap tide and dry season, with two distinct water masses as explained above in 4.1.1 : the upper flowing down-estuary, and the lower flowing up-estuary.

Q_{SED} followed Q_{ADCP} patterns with mean net down-estuary sediment fluxes Q_{SED} 20 times larger in spring tide (0.04 t s^{-1}, Table 2) than in neap tide (0.002 t s^{-1}) in dry season, and with negligible up-estuary sediment fluxes (Q_{SED}-) in wet season lower than 4% of the down-estuary fluxes (Q_{SED}+), both for spring and neap tides. However, the sediment sources are different: while Q_{SED}+ refers to the fluxes of fluvial suspended sediment, Q_{SED}- refers to the upward transport of sediment from the coastal zone or resuspended in the estuary. A main information of the measurements is to quantify this very high up-estuary flow of coastal sediment Q_{SED}- in dry

season and spring tide (0.08 t s^{-1}, Table 2) which is 2/3 of the down-estuary discharge of suspended matter Q_{SED}+ from the river basin (0.12 t s^{-1}). In other words, the estuary is silting up and the delta is consolidating mainly in spring tide during the dry season.

At last, the time variations of tidal amplitude and discharge at Trung Trang during spring tides (both in dry and wet seasons) clearly show that flood tides are shorter than ebb tides in the Van Uc estuary. Such a non linear tidal distortion may be explained either by a high tidal energy dissipation by friction (reflected as a/h= tidal amplitude/water depth) or by a low intertidal storage (measured by V_s/V_c=volume of intertidal storage/volume of channels at mean sea level) (Friedrichs and Aubrey, 1998; Kang and Jun, 2003).

Survey	$\overline{Q_{TT}}$ (m^3 s^{-1})	$\overline{Q_{ADCP}}$ (m^3 s^{-1})	**R^2** (Q_{ADCP}/ Q_{TT})	$\overline{Q_{ADCP}}$ +	$\overline{Q_{ADCP}}$ -	$\overline{Q_{SED}}$ (t s^{-1})	**R^2** (Q_{ADCP}/ Q_{SED})	$\overline{Q_{SED}}$ +	$\overline{Q_{SED}}$ -
WN	2406	ST1: 2352 ST2: 2425 2970 ST3: 1955	0.46	2432	-7	0.34 ST1: 0.33 ST2: 0.35 ST3: 0.35	0.77	0.34	-0.0001
WS	1672	ST1: 2043 ST2: 1757 1841 ST3: 1388	0.81	1832	-74	0.11 ST1: 0.15 ST2: 0.10 ST3: 0.08	0.96	0.11	-0.004
DS	374	478 ST1: 418 ST2: 595 ST3: 420	0.81	1236	-758	0.04 ST1: 0.04 ST2: 0.05 ST3: 0.03	0.94	0.12	-0.08
DN	375	222 ST1: 310 ST2: 148 ST3: 208	0.80	575	-353	ST1: 0.0031 0.002 ST2: 0.0017	0.84	0.006	-0.004

						ST3: 0.0019			

Table 2: Mean water discharges at Trung Trang (Q_{TT}), mean water (Q_{ADCP}) and mean sediment (Q_{SED}) discharges derived from ADCP measurements and corresponding correlation coefficients (R^2), for the four surveys (for our 36 values time series, the 99% significativity threshold is reached for a correlation of 0.42). The means are computed over the 3-days period of each survey (36 values), and computed over 24h when showed for each station (12 values).

4.1.2.2 Spatial variations

Q_{ADCP} measured in the estuary exhibited very small differences compared to the mean discharges from the hydrological station Trung Trang (noted TT from hereafter) in the wet season (below 1% for WN and around 7% for WS, see Table 2). However, in the dry season, Q_{ADCP} is 27% higher than the mean discharge at TT (Q_{TT}) in spring tide, and is 41% lower than Q_{TT} in neap tide. Due to its location roughly 15 km upstream of ST3 (Fig. 1), TT station is less affected than our transect stations by the variation of discharges due to the tides, especially during the dry season, and therefore, discrepancies in measured discharges at our stations and discharges at TT may appear. Overall, time series of Q_{ADCP} and Q_{TT} were highly correlated in surveys WS, DS and DN (R^2=0.80, 0.81 and 0.81 respectively) and only survey WN showed a weaker (but still significant at 99%) average correlation (R^2=0.46) that may be explained by the small amplitudes

of variations in Q_{ADCP} in this season and tidal range. Better correlations were obtained with a lag between Q_{TT} and Q_{ADCP} in surveys WS, DN and DN. The best R^2 values (R^2=0.97, 0.98 and 0.97 for survey WS, DS and DN, respectively) were found at each station and for each survey with a lag of two hours, which indicated that Q_{TT} are leading Q_{ADCP} by two hours all along the estuary, in average, as can be seen in Fig 4. b,c,d.

Increases in Q_{ADCP} of about 52%, 33% and 42 % were observed between ST3 and ST2 during surveys WN, WS and DS, respectively (Table 2). These increases are likely due to water inputs from the Luoc River which flows into the Van Uc River, approximately 2 km downstream of ST3 (see Figure 1). The 40% drop in water discharge that was observed during the survey DN between ST3 and ST2 coincided with decreasing water discharges measured at Trung Trang station (Q_{TT}) during the 3-day period of measurements (Table 2 ; Fig. 4 c), and can thus be explained by a decrease of discharge from the day of ST3 measurements to the day of ST2 measurements. Decreases in water and sediment discharges amplitudes were observed from the river mouth upwards (from ST1 to ST3) during surveys WS, DS and DN (Fig. 4 b,c,d). These decreases could be explained by the variations in the tidal elevation range along the estuary that impact the capability of currents to transport water and sediments. The tidal range increases towards the mouth before decreasing in the river section, when the convergence effects of the estuary sides exceeds the frictional effect of the bed (Dyer, 1995).

Given the scarcity of water discharge data and of their tidal and seasonal variability in the Van Uc river, those values will provide a precious basis for assessing the role of the neap-spring cycle on estuarine dynamics, but will also provide a new benchmark for the calibration/validation of an estuarine hydrodynamic and sediment model.

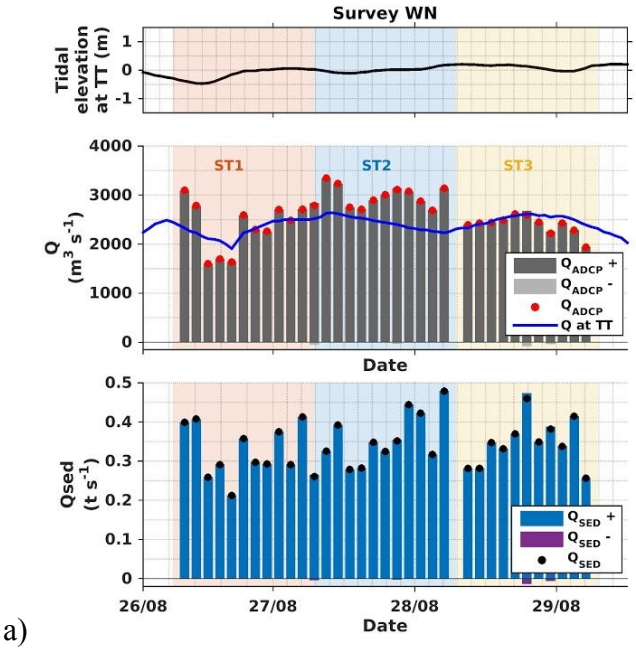
Survey WN
Tidal elevation at TT (m)
ST1
ST2
ST3
Q (m3 s-1)
QADCP +
QADCP -
QADCP
Q at TT
Date
Qsed (t s-1)
QSED +
QSED -
QSED
26/08
27/08
28/08
29/08
Date

a) b)

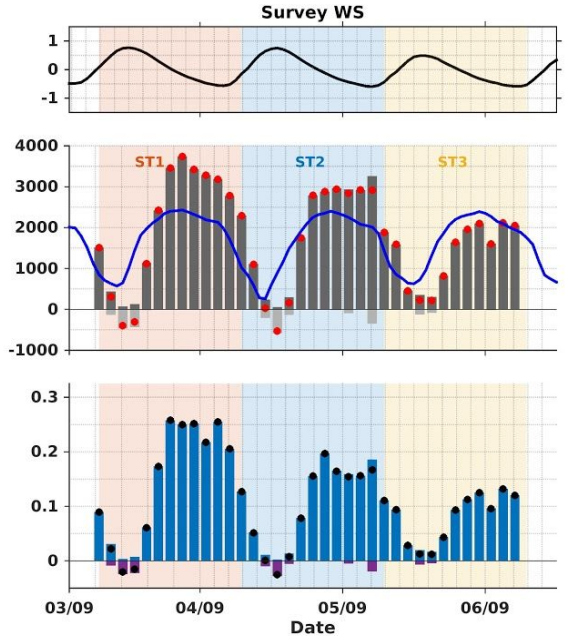
Survey WS
ST1
ST2
ST3
03/09
04/09
05/09
06/09
Date

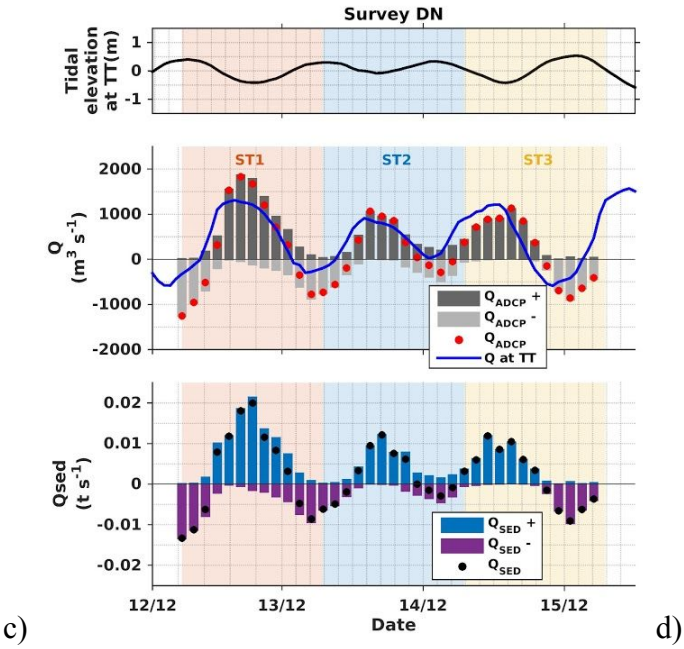

c) d)

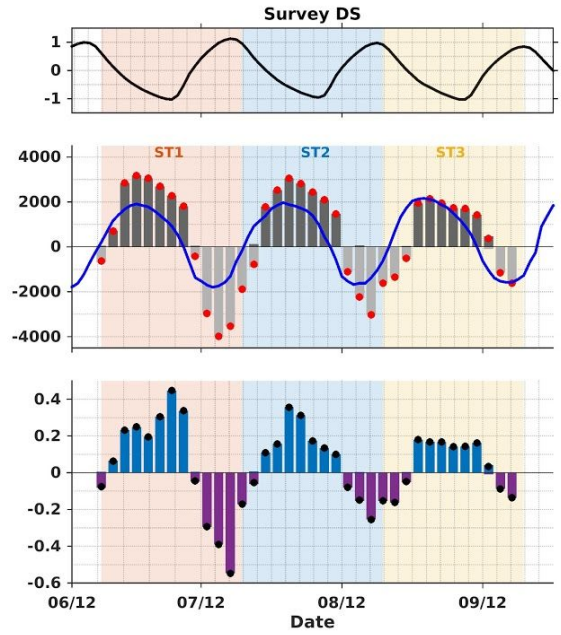

Fig. 4 Tidal elevation (in m, black line) and Q_{TT} (m^3 s^{-1}, blue line), measured Q_{ADCP} (m^3 s^{-1}, red dots) with associated Q_{ADCP}+ and Q_{ADCP}- (dark grey and light grey bars, respectively), and computed Q_{SED} (in t s^{-1}, black dots) with associated Q_{SED}+ and Q_{SED}- (blue and purple bars, respectively), at all three stations for all four surveys.

4.2 Hydrology and turbidity

Salinity as well as Simpson parameter values (Φ), which correspond to the amount of energy needed to homogenize the water column, exhibited large differences between the two seasons. During the wet season, salinity ranged from 0.8 to 1 PSU (not shown) and Φ from 0.07 to 1.3 J m^{-3} (Fig. 5), indicating strictly unstratified fresh waters conditions. During the dry season, salinity ranged from 0.8 to 27 PSU (Fig. 6 a,b) and Φ from 0.1 to 105 J m^{-3} (Fig. 5), which illustrated an oscillation between fresh and unstratified to salty and stratified conditions.

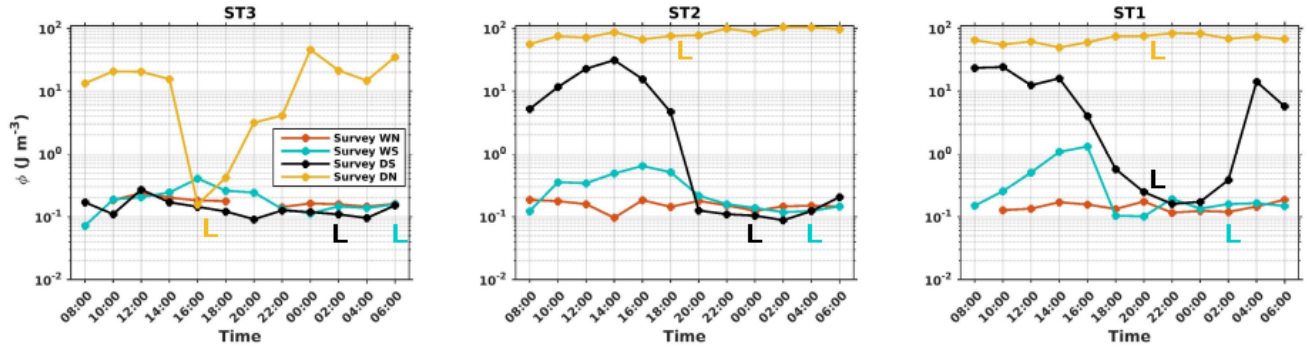

Fig. 5: Simpson parameter values (J m^{-3}) at ST3 (left), ST2 (center) and ST1 (right) for survey WN (orange line), survey WS (cyan line), survey DS (black line) and survey DN (yellow line) during 24h tide cycles. The letters "L" indicate the time of low tide. The missing value at 8pm at ST3 (survey WN) corresponds to a failure in CTD measurement.

During the wet season, tidal and spatial variations of salinity, of the average Richardson gradient number (Ri) and of the Brunt-Vaisala frequency (N^2) were indeed very limited. Values of Ri >0.25 (not shown) indicate that the turbulent mixing across the stratification is suppressed,

therefore the water column is stratified, and conversely Ri < 0.25 indicates a strong vertical mixing. In addition of salinities <1 PSU for WN and WS at all stations, almost all Ri values remained below 0.25 and $N^2 < 0.001\ s^{-2}$ (not shown). Ri <0.25 and homogeneous relatively small values of N^2 are indicative of homogeneous conditions with a strong vertical mixing. However, at 2 pm and 4 pm in survey WS at ST1, Ri=0.52 and 0.64, respectively, and coincided with $\Phi > 1$ (Fig. 5). This light stratification corresponded to a slight increase of the surface water temperatures (of about 1.5 °C, not shown), triggered by an intense solar heating during this particular afternoon.

During the dry season, spatial and tidal variations of salinity, turbidity, Ri and N^2 were high. In spring tides (survey DS), salinity ranges decreased along the estuary from 0.1 to 27 PSU at ST1, from 0.1 to 20 PSU at ST2 and from 0.1 to 0.3 PSU at ST3 (Fig. 6 a). At ST3, the water column remained homogeneous throughout the day, with Ri <0.25 and small homogeneous N^2 values ($<0.001\ s^{-2}$). At ST2 and ST1, the water column alternated between stratified and homogeneous conditions. During low and flood tides, the water column was composed of fresh, turbid (100-250 FTU) and homogeneous waters with Ri <0.25 and $N^2 \sim 0\ s^{-2}$. On the opposite, during high tides and ebb tides, the water column was partly stratified and composed of salty waters with lower turbidity (below 100 FTU). In particular at ST1, Brunt-Vaisälä profiles indicated a stratification near the surface in the top 3 m of the water column with $N^2 \sim 0.05\ s^{-2}$, which coincided with Ri>0.25. At ST2, the intensity of the stratification decreased with Ri< 0.25 and scattered N^2 maxima were observed. Following the results of Fig. 4 d, both spring and diurnal tides played a key role in influencing the water column conditions of the dry season. The water

column was either strictly dominated by fresh turbid riverine waters flowing down-estuary when the tidal amplitude was the lowest, or by salty marine waters flowing up-estuary when the tidal amplitude was high. The tidal intrusion and efficiency to bring salty waters decreased with the distance from the river mouth with a very limited influence at ST3 (20 km upstream of ST1) where the salinity does not exceed 0.3.

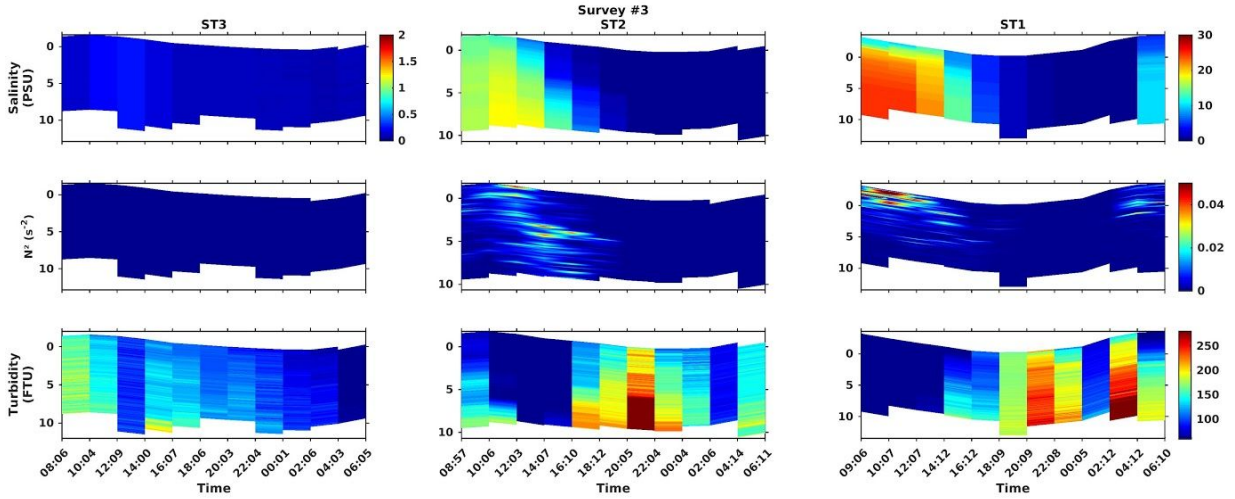

a)

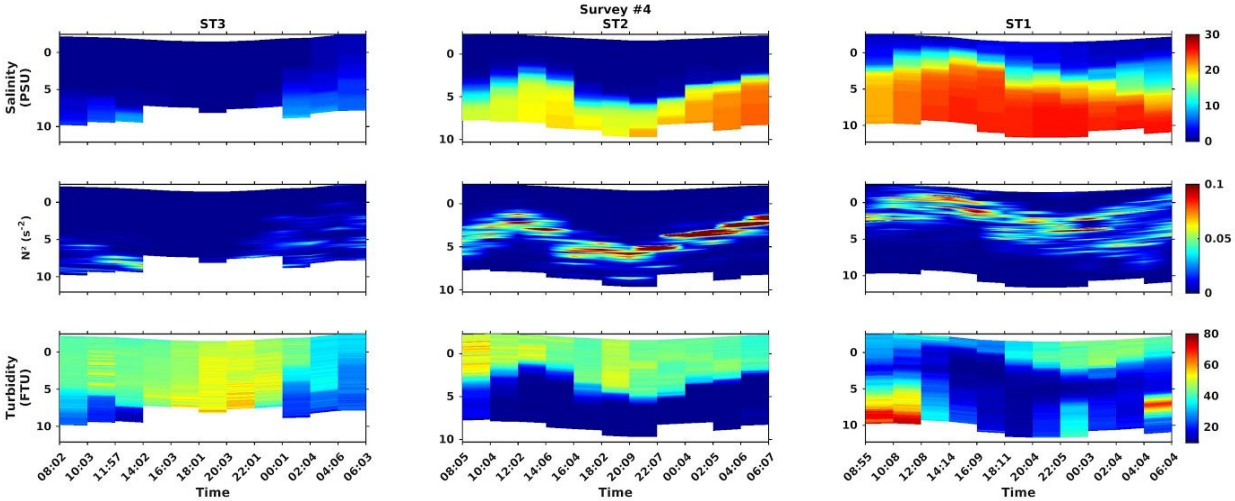

b)

Fig. 6 Salinity (in PSU), N^2 (in s^{-2}), and turbidity (in FTU) temporal series at ST3, ST2 and ST1 measured in survey DS (a, dry season, spring tides) and in survey DN (b, dry season, neap tides). Note the different colorbar for salinity at ST3 for DS, due to very low values, and between DS and DN for N^2 and turbidity

Neap tides water column characteristics in the dry season were very different than spring tides characteristics. At ST1 and ST2, the water column was very stratified and divided into two layers: one bottom layer composed of dense salty waters (up to 25 PSU) and one top layer composed of fresh (~0 PSU) riverine waters (Fig. 6 b). Overall, the turbidity values of survey DN were lower than in any other surveys, but the top layer showed higher turbidity values (40-60 FTU) than the bottom layer (<20 FTU). Similar to survey DS case, the salinity (of the bottom layer) decreased along the estuary with the distance from the mouth (from 0.8 to 27 PSU at ST1, from 0.8 to 23 PSU at ST2 and from 0.8 to 10 PSU at ST3). At ST1 and ST2, N^2 values were maximum in the halocline (~0.1 s^{-2}) and were twice bigger than in survey DS. In addition, Ri >0.25 at ST2 and Ri >0.5 at ST1 indicated a strong stratification, that lasted throughout the 24 hours of measurements. In accordance with the salinity patterns, the stratification intensity decreased along the estuary, with stronger stratification at the stations close to the mouth. As seen in section 4.1.2.2 and in Fig. 4 c, neap tides in the dry season triggered a two layers circulation in the water column. On top, the fresh and turbid river waters flowed downstream (corresponding to Q_{ADCP}+ in Fig. 4 c) whereas, at the bottom the clear salty marine waters flowed upstream (corresponding to Q_{ADCP}- in Fig. 4 c). Lastly, near bed high turbidity values observed at

ST1 were due to particles' resuspension induced by the maximal strength of the upstream flow of high tides (Fig. 6 b).

4.3 Suspended particulate matter

4.3.1 Time variations

The PSDs alternated between bimodal and trimodal distributions from a survey to another, with varying contributions of each particle class to the total particle volume (Fig. 7 a). As mentioned in the literature, PSDs of observed suspensions are more often bimodal or multi-modal rather than unimodal (Ludwig and Hane 1990; Green and Boon, 1993).

In wet season, trimodal PSDs were measured with a first peak for particle diameters < 4 μm, a second peak for particles of diameter 5-10 μm, and a third peak for aggregates of larger diameters (of 30-70 μm for survey WN and of ~30 μm for survey WS). From hereafter, we consider the particles < 4 μm as primary particles (PP), the particles of 4-20 μm as flocculi, and the particles > 20 μm as microflocs. In the wet season, spring tides likely induced stronger turbulent stresses than neap tides (see Fig. 4b as compared to 4a) that may cause a breakage of the largest particles, hence a decrease in populations of microflocs > 30 μm in spring tides. This is consistent with the results from Mikkelsen et al. (2006), who demonstrated that when the water column stress increases, the volume occupied by large particles (in their case : macroflocs) decreases, while the volume occupied by finer particles (in their case : microflocs) increases.

In dry season, bimodal PSDs were measured with peaks moving in the spring-neap tide cycle. Peaks of PP and flocculi were observed in spring tides (survey DS, Fig. 7 a), while peaks of flocculi and microflocs appeared in neap tides (survey DN). However, the tidal average PSDs in spring tides masked a diurnal alternation of PSDs. At low tide (Fig. 7 b), the instant PSD was similar to the average PSD of survey DS (Fig. 7 a) but at high tide, the instant PSD (Fig. 7 b) appeared to be similar to the PSDs of survey DN (Fig. 7 a). These observations highlight the fact that riverine waters, which dominated the water column around low tides in spring tide (see section 4.1.2.2, Fig. 4 d and section 4.2.2, Fig. 6 a), carried PP and flocculi. On the other side, marine salty waters, which dominated the water column around high tide in spring tides and all along neap tides, carried flocculi and microflocs. We suggest that the microflocs were formed by salinity-induced flocculation of PP or covarying aggregation by bio-processes, either within the estuary, or in the coastal area and they were brought back into the estuary by the tidal advection. As seen in section 4.2.2 and Fig. 6 a,b, salinity maxima oscillated between 0.8 and 27 PSU during the dry season, and Vinh et al. (2018) showed that flocculation happened for salinity as low as 0.1 PSU in the Cam Nam estuary (Fig. 1). Besides, Eisma (1993) indicated that salinity flocculation is complete at 8 PSU or less, and Mari et al. (2012) demonstrated that the stickiness properties of organic exopolymeric substances increase between 10 and 15 PSU, enhancing the bio-induced flocculation in the Cam Nam estuary.

It is important to note that the high concentrations of PP observed in almost all surveys and which sometimes corresponded to 5-15 % of the SPMVC, are to be considered with caution. Rather than providing an exact number, these concentrations should be interpreted as an

indication of the presence of very fine particles (Fettweis and Baeye, 2015). Indeed, the LISST-100X (type B) detectors show some limitations and uncertainties related to the characteristics of the particles. Significant concentrations of particles smaller than the lowest LISST detection limit (<1.25 μm) can influence the entire PSD with increase of concentrations of the two smallest size classes, a decrease of the next classes and an increase on the largest size classes (Andrew et al., 2010; Graham at al., 2012).

4.3.2 Spatial variations

We further investigated the transfer of particles from a class to another, and the relative contribution of each class to the total SPMVC (Fig. 7 c). During spring tides (surveys WS and DS), the proportion of each class remained quite unchanged along the estuary, while longitudinal variations were observed in neap tides (surveys WN and DN), with decreasing proportion of primary particles and increasing proportion of microflocs from upstream (ST3) to the river mouth (ST1). In survey WN, for example, microflocs made up 23% of the total volume at ST3, 35% at ST2 and 39% at ST1, while PP contribution to SPMVC decreased from ST3 (34%) to ST2 (22%) and ST1 (18%). Similar longitudinal transfers from PP to microflocs were observed in survey DN, even though the PP contributions to SPMVC were about twice larger in survey WN. These discrepancies in PP concentrations between dry and wet seasons could be due to differences in sediments discharges (Q_{SED}) between the seasons (section 4.1.2.1), with mean Q_{SED} approximately 170 times bigger in survey WN than in DN (Table 2). In survey DN, salinity-induced flocculation may explain the transfers of PP to microflocs (see previous

section), intensifying closer to the river mouth (ST2 and ST1). For spring tide surveys (DS and WS), the proportion of each class remained spatially almost unchanged because the along-estuary salinity gradient was non-existent, limiting the flocculation and therefore the transfer of PP to microflocs.

Lastly, the SPMVC progressively decreased along the estuary with higher volume concentrations recorded at ST3 than at ST2 and ST1, in each case (see the values on Fig. 7 a). The volume concentration ratio between ST3 and ST1 decreased from 12 for survey WN, to ~3 for surveys WS, DS and DN. Although SPMVCs should not be considered as exact values but only as indicators, such a volume loss may be explained by particles deposition, with zones of accumulation spanning from ST3 to ST1. Here, hydrodynamical-sediment transport modelling would be a useful tool to detail the transport and deposition of SPM, and could highlight zones of accumulation / accretion in the estuary and along the shorelines.

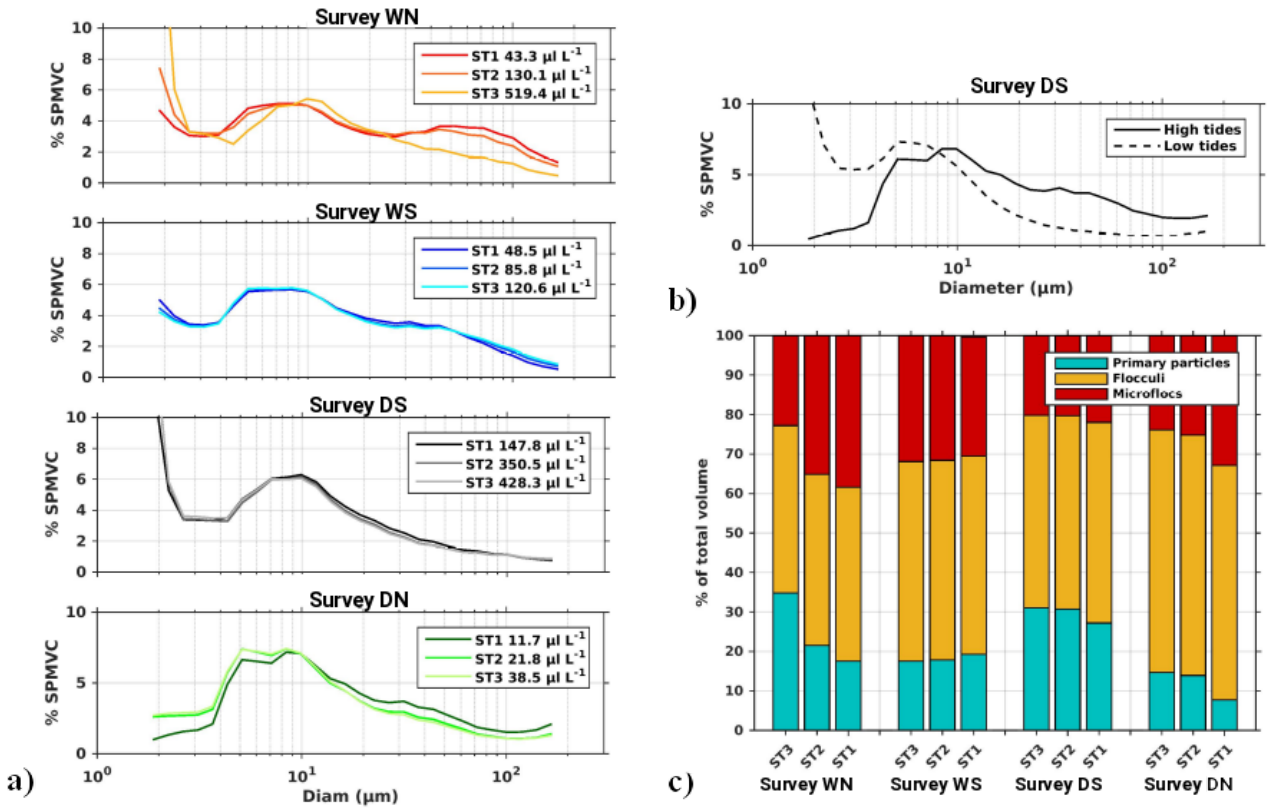

Fig. 7 a) PSD at each station for all surveys and their associated SPMVC. b) PSD at ST2 in survey DS at high tide (measured at 8 am) and low tide (measured at 8 pm). c) Proportions of primary particles, flocculi and microflocs in terms of % of volume occupied, by station and for all four surveys.

5. Discussion and Conclusion

Water column and sediment time-series observations made along the lowermost 20 km of the Van Uc river, which included acoustic and optical determination of SPM concentration, measurements of flow velocity, salinity, and PSD, at different seasons and neap-spring cycle, showed that:

1 - The water and sediment discharges of the Van Uc river undergo a comprehensive regime change between high-seasonal (wet season) and low-seasonal (dry season) discharges. The estuary varied from mixed to stratified, depending on tidal state and freshwater inflow. Strictly mixed conditions occurred during high-flow season. Water column conditions transited from mixed, partly-stratified to very stratified during low-flow season, due to the combined effects of neap-spring cycle, diurnal tides and low discharges: in spring tides, the water column was either partly-stratified near the surface with high tides or mixed with low tides, while neap tides triggered a constant and strong stratification.

2 - The seasonal discharges are affected by the neap-spring cycle with different effects between the seasons. The high seasonal flow is not disrupted by neap tides but spring tides can reverse the downstream river flow at high tides. In low-flow season, the spring tides reverse the flow for half the day, while neap tides trigger a gravitational circulation (two layer circulation) with a flow in both directions (up-estuary for the bottom layer and down-estuary for the top layer) and a very stratified water column. The occurrence of gravitational circulation thus depends both on freshwater flow and on the tidal state.

3- Decomposition of the suspended matter flux revealed that the riverine down-estuary component was the most important during high flow season while gravitational and tidal processes, like local resuspension, were most important during low flow season. Up-estuary suspended matter flux appeared to account for ⅔ of the down-estuary flux in the low-flow season, which indicates that the estuary is silting up and the delta is consolidating mainly in the dry season. This fine marine sediment import in the estuary, likely due to a gravitational circulation, is driven by the longitudinal density gradient caused by freshwater inflow,

developing an estuarine turbidity maximum near the upstream boundary of the gravitational circulation (Dronkers 1986). This is particularly observable in neap tides when a sediment flux is oriented seaward in a surface layer at the same time than a landward sediment flux in the underlying salted layer. The ETM (estuarine turbidity maximum) was described by Vinh et al. (2018) in another distributary of the Red River, close to the Van Uc River, and our measurements indicates that an ETM is likely located between stations ST1 and ST2 in dry season. In wet season, salinity remained very low in the riverine part of the estuary (with maximum value of 0.09 PSU at the river mouth), indicating that mixing between riverine and marine waters develops in the bay and in coastal waters, like in the Cam-Nam Trieu estuary (Vinh et al., 2018). Since stratification remains low during the tidal cycle, another process than gravitational circulation should explain the landward flux of suspended sediment in the wet season, which was observed at spring tides. Important asymmetry (or distortion) can occur in the tidal curve and velocities, in estuaries characterized by larger tidal ranges than water depths and by cross-river sections rapidly decreasing going up-estuary (Dyer, 1986). In these cases, flood tides become shorter and stronger than ebb tides. The distortion of the tide wave in spring tide may be the dominant process to explain the up-estuary sediment mobility in wet season at spring tide during flood. A combination of the two main estuarine processes could thus explain the estuarine behaviour between two extreme conditions, at neap tides in dry season when gravitational circulation dominates, and at spring tides in wet season, when tidal distortion dominates. The effects of both processes may be further quantified and compared from numerical simulations.

4- Seasonal and tidal flow dynamics are also reflected in grain-size characteristics. All types of particles (PP, flocculi and microflocs) are transported during the high-flow season at any tidal stages, while mainly flocculi and microflocs are transported in the low-flow season, at high tides in spring tides and all along neap tides. The presence of the finest fraction (PP and flocculi) corresponds to the so-called wash load transport, which keeps particles in motion by turbulence at all current speeds and can therefore occur at any season and any tidal stages. The coarser fraction (microflocs) is likely in motion and transported by suspension, re-suspension and bedload (Dyer, 1995). While suspension can occur at any season, bedload occurs mostly during the high-flow season with highest current velocities (high water discharges).

This study took place in the framework of a more comprehensive modeling project which aims at representing the transport and fate of sediment from the Red River to the Gulf of Tonkin and analyzing the relevant processes. As tides have a major effect on the sediment dynamics within the estuaries and in the plume area (Pritchard 1954, 1956; Allen et al., 1980; Fontes et al., 2008; Vinh et al., 2018), and as monsoonal estuaries are highly affected by seasonal water discharges (Wolanski et al., 2013; Vinh et al., 2014; Nowacki et al., 2015), it is necessary to document and understand the estuarine hydrology and suspended matter dynamics, before setting up a set of numerical models and investigating the fine scale sediment physics. This study complemented the understanding of the Van Uc estuary, which, to our knowledge, has never been sampled before. Further studies are also encouraged to focus on the mixing processes and estuary configuration in wet season along the Red River delta.

Acknowledgments

This paper is a contribution to the LOTUS International Joint Laboratory (lotus.usth.edu.vn). The authors warmly thank Gaël Orban de Xivry and Pablo Lipchitz for their precious work and help during the field campaigns, as well as the boat crew.

Authors Contribution

VP, SO and MH conceived the study. VP, VDV, SO and MH organized the field trip, and VP and VDV performed the measurements. VP, SO and GM analyzed the data. VP and SO prepared the manuscript with contributions of GM, MH and PM.

Conflicts of Interest

The authors declare no conflict of interest.

References

Aminot, A., and R. Kérouel. 2004. Hydrologie des écosystèmes marins: paramètres et analyses. Editions Quae.

Andrew, S., D. Nover, S. Schladow. 2010. Using laser diffraction data to obtain accurate particle size distributions: The role of particle composition, *Limnol. Oceanogr. Methods* 8: 507-526, doi:10.4319/lom.2010.8.507.

Carmeron, W. M., and D. Pritchard. 1963. *Estuaries,* The sea, 2: 306-324, Wiley, New York.

Chapalain, M., R. Verney, M. Fettweis, M. Jacquet, D. Le Berre, P. Le Hir. 2018. Investigating suspended particulate matter in coastal waters using the fractal theory. *Ocean Dynamics* 69 (1): 59-81. http://doi.org/10.1007/s10236-018-1229-6.

Deines, K.L. 1999. Backscatter estimation using broadband ADCP. R.D. Instruments. Application Note FSA-008.

Ding, Y., C. Chen, R. C. Beardsley, X. Bao, M. Shi, Y. Zhang, Z. Lai, R. Li, H. Lin and N. T. Viet. 2013. Observational and model studies of the circulation in the Gulf of Tonkin, South China Sea. *J. Geophys. Res. Oceans* 118: 6495-6510. doi: 10.1002/2013/JC009455.

Downing, J. 2006. Twenty-five years with OBS sensors: The good, the bad, and the ugly. *Cont. Shelf Res.* 26: 2299-2318. doi:10.1016/j.csr.2006.07.018.

Dronkers, J. 1986. Tide-induced residual transport of fine-sediment. In *Physics of shallow estuaries and bays, Lecture notes on coastal and estuarine studies.* Vol. 16: 228-244.

Dyer, K. 1986. *Coastal and Estuarine Sediment Dynamics*. John Wiley and Sons, Chichester.

Dyer, K. 1995. Chapter 14 Sediment transport processes in estuaries. In: G.M.E, Perillo (Ed.) Developments in Sedimentology, Geomorphology and Sedimentology of Estuaries. Elsevier, pp: 423-449. https://doi.org/10.1016/S0070-4571(05)80034-2

Eisma, D. 1993. *Suspended Matter in the Aquatic Environment*. Springer: Berlin, Germany.

Fang, G., Y. K. Kwok, K. Yu and Y. Zhu. 1999. Numerical simulation of principal tidal constituents in the South China Sea, Gulf of Tonkin and Gulf of Thailand. *Cont. Shelf Res.* 19(7): 845-869. https://doi.org/10.1016/S0278-4343(99)00002-3 .

Fettweiss, M. and M. Baeye. 2015. Seasonal variation in concentration, size, and settling velocity of muddy marine flocs in the benthic boundary layer, *J. Geophys. Res. Oceans* 120: 5648-5667. doi:10.1002/2014JC010644.

Fontes, R. F. C., B. M. Castro and R. C. Beardsley. 2008. Numerical study of circulation on the inner Amazon Shelf, *Ocean Dyn.* 58:187-198. https://doi.org/10.1007/s10236-008-0139-4.

François, R.E. and G. R. Garrison. 1982a. Sound absorption based on ocean measurements: Part I: Pure water and magnesium sulfate contributions. J. *of the Acoust. Soc. of Amer.* 72: 896-907. doi: 10.1121/1.388170.

François, R.E. and G.R. Garrison. 1982b. Sound absorption based on ocean measurements: Part II: Boric acid contribution and equation of total absorption. *J. of the Acoust. Soc. of Amer.* 72: 1879-1890. doi: 10.1121/1.388673.

Friedrichs, C.T., D. G. Aubrey. 1988. Non-linear tidal distorsion in shallow well-mixed estuaries: a synthesis. *Est. Coast. Shelf Sci.* 27: 521-545. doi:10.1016/0272-7714(88)90082-0

Fugate, D. C., C. T. Friedrichs. 2002. Determining concentration and fall velocity of estuarine particle populations using ADV, OBS and LISST, *Cont. Shelf Res*. 22: 1867-1886. https://doi.org/10.1016/S0278-4343(02)00043-2

Gartner, J. W. 2002. Estimation of suspended solids concentrations based on acoustic backscatter intensity: theoretical background, Turbidity and other sediment surrogates workshop, Reno, Nevada.

Gartner, J. W. and Cheng R. T. 2001. The promises and pitfalls of estimating total suspended solids based on backscatter intensity from acoustic Doppler current profilers. Proceedings 7th Federal Interagency Sedimentation Conference, III-119-III-126, Reno, Nevada.

Geyer, W. R. and P. MacCready. 2014 The Estuarine Circulation, *Annu. Rev. Fluid Mech.* 46: 175-97. doi: 10.1146/annurev-fluid-010313-141302.

Geyer, W. R., J. H. Trowbridge and M. M. Bowen. 2000. The dynamics of a partially mixed estuary, *J. Phys. Oceanogr.*, 30: 2035-2048. https://doi.org/10.1175/1520-0485(2000)030<2035:TDOAPM>2.0.CO;2

Graham, G. W., E. J. Davies, W. A. M. Nimmo-Smith, D. G. Bowers and K. M. Braithwaite. 2012 Interpreting LISST-100X measurements of particles with complex shape using digital in-line holography, *J. Geophys. Res.* 117: C05034. doi: 10.1029/2011JC007613.

Green, M. O. and J. D. Boon III. 1993. The measurement of constituent concentrations in non-homogeneous sediment suspensions using optical backscatter sensors. *Mar. Geol.*: 110: 73-81. https://doi.org/10.1016/0025-3227(93)90106-6

Ha, H. K., J. -P. Y. Maa, K. Park and Y. H. Kim. 2011. Estimation of high-resolution sediment concentration profiles in bottom boundary layer using pulse-coherent acoustic doppler current profilers, *Mar. Geol.* 279: 199-209. doi:10.1016/j.margeo.2010.11.002.

Jay, D. A., K. Leffler, H. L. Diefenderfer and A. B. Borde. 2014 Tidal-fluvial and estuarine processes in the lower Columbia River: I, a long-channel water level variations, Pacific ocean to Bonneville Dam, *Estuar. Coasts* 38: 415-433. doi: 10.1007/s12237-014-9819-0.

Jay, D. A. and J. D. Smith. 1990. Residual circulation in shallow estuaries: 1. Highly stratified, narrow estuaries, *J. Geophys. Res.* 95: 711. https://doi.org/10.1029/JC095iC01p00711

Kang, J.W. and K. S. Jun. 2003. Flood and ebb dominance in estuaries in Korea. *Est. Coastal Shelf Sci.* 56: 187-196. doi:10.1016/S0272-7714(02)00156-7.

Kim, Y. H., G. Voulgaris. 2003 Estimation of suspended sediment concentration in estuarine environments using acoustic backscatter from ADCP (source: http://www.rdinstruments.com/pdfs/Kim_Yong.pdf). Accessed 17 January 2019.

Kirinus, E. W., J. C. da Costa and E. H. Leão Fernandes. 2012 The contribution of waves in mixing processes of the Patos Lagoon plume. *Int. J. Geosci.* 3: 1019-1026. doi:10.4236/ijg.2012.35102

Lai, W., J. Pan and A. T. Devlin. 2018 Impact of tides and winds on estuarine circulation in the Pearl River Estuary, *Cont. Shelf. Res.* 168: 68-82. https://doi.org/10.1016/j.csr.2018.09.004.

Le, T. P. Q., J. Garnier, G. Billen, S. Théry and V. M. Chau. 2007. The changing flow regime and sediment load of the Red River, Viet Nam. *J. Hydrol.* 334: 199-214, doi:10.1016/j.jhydrol.2006.10.020

Le Hir, P., F. Cayocca and B. Waeles. 2011. Dynamics of sand and mud mixtures : A multiprocess-based modelling strategy. *Cont. Shelf Res.* 31: 135-149. doi :https://doi.org/10.1016/j.csr.2010.12.009

Lefebvre, J. P., S. Ouillon, V. D. Vinh, R. Arfi, J. Y. Panché, X. Mari, C. V. Thuoc and J. P. Torréton. 2012. Seasonal variability of cohesive sediment aggregation in the Bach Dang-Cam Estuary, Haiphong (Vietnam). *Geo.-Mar. Lett.* 32: 103-121. doi: 10.1007/s00367-011-0273-8.

Ludwig, K. A. and D. M. Hanes. 1990. A laboratory evaluation of optical basckscatterance suspended solids sensors exposed to sand-mud mixtures. *Mar. Geol.* 94: 173-179. https://doi.org/10.1016/0025-3227(90)90111-V

Lurton, X. 2002. Utilisation des ADCP pour la mesure de particules en suspension: synthèse des aspects acoustiques. IFREMER (France). Laboratory report, pp 29.

Mari, X., J. P. Torréton, V. T. Chu, J. P. Lefebvre and S. Ouillon. 2012. Seasonal aggregation dynamics along a salinity gradient in the Bach-Dang estuary, North Vietnam. *Estuar. Coast. Shelf Sci.* 96: 151-158. https://doi.org/10.1016/j.ecss.2011.10.028

Marsaleix, P., F. Auclair, J. W. Floor, M. J. Herrmann, C. Estournel, I. Pairaud and Ulses C. 2008 Energy conservation issues in sigma-coordinate free-surface ocean models. *Ocean Modell.* 20(1): 61-89. http://dx.doi.org/10.1016/j.ocemod.2007.07.005

Meybeck, M. 1993. Riverine transport of atmospheric carbon: sources, global typology and budget. *Water Air Soil Pollut.* 70(1-4): 443-463. https://doi.org/10.1007/BF01105015.

Miranda, L. B., B. M. de Castro and B. Kjerfve. 2002. Princípios de oceanografia física de estuários. *São Paulo: EDUSP* 414.

Mikkelsen, O. A., T. G. Milligan, P. S. Hill., R. J. Chant, C.F. Jago, S. E. Jones, V. Krivtsov and G. Mitchelson-Jacob (2008) The influence of schlieren on in situ optical measurements used for particle characterization. *Limnol. Oceanogr. Methods* 6: 133-143. https://doi.org/10.4319/lom.2008.6.133.

Mikkelsen, O. A., P. S. Hill and T. G. Milligan. 2006. Single-grain, microfloc and macrofloc volume variations observed with a LISST-100 and a digital floc camera. *J. Sea Res.* 55: 87-102. doi: 10.1016/j.seares.2005.09.003.

Mikkelsen, O. A., P. S. Hill, T. G. Milligan and R. J. Chant. 2005. In situ particle size distributions and volume concentrations from a LISST-100 laser particle sizer and a digital floc camera. *Cont. Shelf Res.*, 25 (16), 1959-78. doi: 10.1016/j.csr.2005.07.001.

Milliman, J. D. 1991. Flux and fate of fluvial sediment and water in coastal seas. In: Mantoura R.F.C., Martin J.-M., Wollast R. (eds) Ocean Margin Processes in Global Change, John Willey and Sons Ltd., Chichester, 69-89.

Milliman, J.D. and R. H. Meade. 1983. World-wide delivery of river sediment to the oceans. *J. Geol.* 91: 1-21. https://doi.org/10.1086/628741

Mueller, D. S., C. R. Wagner, M. S. Rehmel, K. A. Oberg and F. Rainville. 2013. Measuring discharge with the Acoustic Doppler Current Profilers from a moving boat (ver 2.0, December 2013): U.S. Geological Survey Techniques and Methods, 3, (A22): 95. http://dx.doi.org/10.3133/tm3A22/

Mullison J. (2017) Backscatter estimation using broadband Acoustic Doppler Current Profilers - Updated. Presented at the ASCE Hydraulic Measurements & Experimental Methods Conference, Durham, NH.

Pacanowski, R. C., and S. G. H. Philander (1981) Parameterization of vertical mixing in numerical models of tropical oceans. *Journal of Physical Oceanography* 11 (11): 1443-51. *https://doi.org/10.1175/1520-0485(1981)011<1443:POVMIN>2.0.CO;2*

Pritchard, D. W. 1954. A study of the salt balance in a coastal plain estuary. *J. Mar. Res.* 13(1): 133-144.

Pritchard, D. W. 1956. The dynamic structure of a coastal plain estuary. *J. Mar. Res.* 15: 33-42.

Priya, K. L., P. Jegathambal and E. J. James. 2012. Hydrodynamic modelling of estuaries a-state-of-art. *Int. J. Environ. Sci.* 3: 223-240. doi:10.6088/ijes.2012030131024.

Rouhnia, M., A. Keyvani and K. Storm. 2014. Do changes in the size mud flocs affect the acoustic backscatter values recorded by a Vector ADV? *Cont. Shelf. Res.* 84: 84-92. doi:10.1016/j.csr.2014.05.015.

Simpson, J. H., C. M. Allen and N. C. G. Morris. 1978. Fronts on the continental shelf. *J. Geophys. Res.* 83: 4607-14.

Simpson, J. H., J. Brown, J. Matthews and G. Allen. 1990. Tidal straining, density currents, and stirring in the control of estuarine stratification. *Estuaries* 13: 125-132. https://doi.org/10.2307/1351581

Styles, R. 2006. Laboratory evaluation of the LISST in a stratified fluid. *Mar. Geol.* 227: 151-162. doi: https://doi.org/10.1016/j.margeo.2005.11.011.

Tessier, C. (2006) Caractérisation et dynamique des turbidités en zone côtière: l'exemple de la région marine Bretagne Sud. PhD thesis. Université de Bordeaux 1.

Thorne, P. D., C. E. Vincent, P. J. Hardcastle, S. Rehman and N. D. Pearson. 1991. Measuring suspended sediment concentrations using acoustic backscatter devices. *Mar. Geol.* 98: 7-16. https://doi.org/10.1016/0025-3227(91)90031-X

Turner, J. S. 1973. Buoyancy effects in fluids. Cambridge University.

Uncles, R. J. and J. A. Stephens. 1996. Salt intrusion in the Tweed Estuary. *Est. Coast. Shelf Sci.* 43: 271-273. https://doi.org/10.1006/ecss.1996.0070.

Unesco. 1983. Algorithms for computation of fundamental properties of seawater. Unesco.

Van Maren, D. S. 2007. Water and sediment dynamics in the Red River mouth and adjacent coastal zone. *J. Asian Earth Sci.* 29: 508-522. https://doi.org/10.1016/j.jseaes.2006.03.012.

Vietnam maritime administration (Vinamarine). Approved planning for dredging in Hai Phong port. Available online: http://vinamarine.gov.vn (accessed on 10 January 2019).

Vinh, V. D., S. Ouillon, T. D. Tanh, V. L and Chu. 2014. Impact of the Hoa Binh dam (Vietnam) on water and sediment budgets in the Red River basin and delta. *Hydrology and Earth System Sciences* 18: 3987–4005. doi:10.5194/hess-18-3987-2014

Vinh, V. D., S. Ouillon and V. U. Dinh. 2018. Estuarine Turbidity Maxima and Variations of Aggregate Parameters in the Cam-Nam Trieu Estuary, North Vietnam, in Early Wet Season. *Water* 68: 1-33. doi: 10.3390/w10010068.

Voulgaris, G. and S. Meyers. 2004. Temporal variability of hydrodynamics, sediment concentration and sediment settling velocity in a tidal creek. *Cont. Shelf Res.* 24: 1659-1683. doi:10.1016/j.csr.2004.05.006.

Wei, X., S. Sauvage, T. P. Q. Le, S. Ouillon, D. Orange, V. D. Vinh and J. -M Sanchez-Perez. 2019. A Modeling Approach to Diagnose the Impacts of Global Changes on Discharge and Suspended Sediment Concentration within the Red River Basin. *Water* 11: 958. doi:10.3390/w11050958

Wolanski, E., F. Andutta and E. Delhez. 2013. Estuarine Hydrology. In Bengtsson L., Herschy R. W., Fairbridge R. W. (eds) Encyclopedia of Lakes and Reservoirs, Encyclopedia of Earth Sciences. 238-249. doi: 10.1007/978-1-4020-4410-6_77.

Wyrtki, K. 1961. Physical oceanography of the Southeast Asian waters. Naga Rep. 2, 195 pp. [Available from: https://escholarship.org/uc/item/49n9x3t4].

Zu, T., J. Gan, S. Y. Erofeeva. 2008. Numerical study of the tide and tidal dynamics in the South China Sea. *Deep-Sea Res*. I 55: 137–154. doi:10.1016/j.dsr.2007.10.007